A method for remote sensing of weak planetary magnetic fields: Simulated application to Mars

Richard Larsson,[1] Robin Ramstad,[2] Jana Mendrok,[1] Stefan Alexander Buehler,[1] and Yasuko Kasai[3]

Received 3 July 2013; revised 12 September 2013; accepted 13 September 2013; published 1 October 2013.

[1] We present a method for characterizing the magnetic anomalies from the crustal fields in the lower atmosphere of Mars that requires two perpendicular linear polarization measurements of the Zeeman effect. The maximum effect of the magnetic field on the signal is found at the Doppler broadening width at low pressures rather than at the magnetically induced line frequency shift, and the effect strongly increases with increasing magnetic field strength. Based on simulations of the Zeeman-affected spectral cross section of the 119 GHz O_2 line in a model Martian atmosphere at various magnetic field strengths, we conclude that it should be possible to probe the strength of the magnetic anomalies remotely with presently available technology. We discuss limitations of the method, how these results could be relevant to the interpretation of residuals in Herschel/HIFI observations of Mars, as well as the application to detection of exoplanetary magnetic fields. **Citation:** Larsson, R., R. Ramstad, J. Mendrok, S. A. Buehler, and Y. Kasai (2013), A method for remote sensing of weak planetary magnetic fields: Simulated application to Mars, *Geophys. Res. Lett.*, *40*, 5014–5018, doi:10.1002/grl.50964.

1. Introduction

[2] The fields of crustal magnetization on the Martian southern hemisphere are thought to be remnants of an ancient dynamo-driven planetwide magnetic dipole. This Martian dynamo likely ceased to function when the planet's mantle solidified, decreasing the heat flux from the core. Orbital measurements by the magnetometer on Mars Global Surveyor, taken 100–400 km above the surface, have revealed the influence of the fields which predominate the southern hemisphere [*Brain et al.*, 2003; *Haider et al.*, 2011]. However, the influence of a varying solar wind flux and interplanetary magnetic field angle, with corresponding variations in the induced magnetosphere, as well the complexity of the fields, makes it difficult to accurately estimate the field intensities at the surface. According to *Brain et al.* [2003], the best fit of a power law function to the data implies a surface strength of ∼15,800 nT over the strongest source but is dependent on assumed source depths. Furthermore, weaker fields may cover significant surface areas and hence atmospheric volumes. A detailed map of the near-surface crustal field may help constrain when and how the magnetic dipole ceased to function, in turn, maybe shed some light on the present topographical and magnetic dichotomy [*Citron and Zhong*, 2012]. At the time of writing, there has been no functioning lander with a magnetometer instrument on board that can do in situ measurements at the surface. Even if such an instrument was to be placed on a future lander, it would only be able to cover a single or a small range of positions on the surface.

[3] The presence and strength of a planet's intrinsic magnetic field strongly affects its interaction with the solar wind, which in turn influences the rate of atmospheric escape [*Haider et al.*, 2011; *Lundin et al.*, 2011]. A prominent example is the planet-wide dipole field of Earth that shields the entire planet from the solar wind, except for the auroral oval where a polar outflow of ionospheric ions forms. The ionospheric ions partly escape the planet, but a large portion of the outflow is recycled in the plasmasphere and plasma sheet systems [*Seki et al.*, 2001]. Analogous recycling in "mini-magnetospheres" formed by the Martian magnetic anomalies are thought by *Lundin et al.* [2011] to be the reason for fewer ions reaching the Martian magnetotail from the southern hemisphere compared to the northern hemisphere, which was also observed by *Nilsson et al.* [2011]. Outside the magnetized regions, the atmosphere is only protected by an induced magnetospheric boundary resulting from currents induced in response to the magnetic field frozen into the solar wind [e.g., *Barabash et al.*, 2007].

[4] By preventing atmospheric escape, this shielding effect by an intrinsic magnetic field influences the long-term habitability of the planet. The terrestrial planets are generally thought to have featured similar atmospheric conditions at their formation; however, only Earth has retained an active hydrological cycle thought necessary for life [*Hunten*, 1993; *Kasting*, 1993]. With the ongoing discoveries of potentially habitable exoplanets [e.g., *Selsis et al.*, 2007], it is thus crucial to remotely detect exoplanetary magnetic fields as such feature seems to be closely linked to its potential for habitability.

[5] With Mars as proxy for weakly magnetized planets, we aim to show how spectroscopic observations of the Zeeman splitting of the 119 GHz O_2 line by planetary magnetic fields can perform this remote detection. Similar methods, but for stronger (∼6 orders of magnitude) magnetic fields, are utilized in stellar physics to characterize the magnetic field of stars [e.g., *Berdyugina and Solanki*, 2002]. However, the authors are not aware of any previous works utilizing

Additional supporting information may be found in the online version of this article.

[1]Division of Space Technology, Luleå University of Technology, Kiruna, Sweden.
[2]Swedish Institute of Space Physics, Kiruna, Sweden.
[3]National Institute of Information and Communications Technology, Tokyo, Japan.

Corresponding author: R. Larsson, Division of Space Technology, Luleå University of Technology, Kiruna, Sweden. (ric.larsson@gmail.com)

0094-8276/13/10.1002/grl.50964

the described method for characterizing weak planetary magnetic fields.

2. Method

[6] We will here describe a method by which two polarized passive microwave spectrometers, with sufficiently high-frequency resolutions, can retrieve the magnetic field information from an atmosphere. Commonly known as the Zeeman effect, the physical phenomenon utilized is the splitting of certain lines in frequency as a function of the magnetic field. Only the most basic aspects of the theory of the Zeeman effect, the theory of line shapes, and polarized radiative transfer are discussed herein. We refer to previous work (R. Larsson et al., A treatment of the Zeeman effect using Stokes formalism and its implementation in the Atmospheric Radiative Transfer Simulator ARTS, accepted by *Journal of Quantitative Spectroscopy and Radiative Transfer*, 2013) for a more thorough description of the model and for derivation of all unreferenced quantities that follows in this work. The Zeeman effect on Earth atmospheric radiative transfer has been modeled for quite a while [*Lenoir*, 1967], but only recently have measurements become more regular as modern instruments are able to resolve the effect [*Hartmann et al.*, 1996; *Schwartz et al.*, 2006]. The method can be simplified to stating that the difference between two perpendicularly polarized signals after transfer through a planetary atmosphere may contain information about the planetary magnetic field.

2.1. The Zeeman Effect Signal

[7] The Zeeman effect can be described as a perturbation theory applied to transitions with a nonzero sum electron spin in an external magnetic field. Instead of an unperturbed line center for the transition, there are instead several frequency-shifted, or perturbed, line centers with the same total line strength. The shift from the unperturbed line center is proportional to the strength of the magnetic field. In addition, these lines are associated with specific polarizations depending on the direction of the magnetic field. If the propagation direction of the radiation is perpendicular to the magnetic field, the Zeeman effect changes the linear polarization components. If the propagation direction of the radiation is parallel to the magnetic field, the Zeeman effect changes the circular polarization components. For other propagation directions relative to the magnetic field, the Zeeman effect mixes the above extrema. Furthermore, in the general case, the polarization around the perturbed line centers is rotated due to a difference in propagation speed between the different polarization directions [*Jefferies et al.*, 1989].

[8] In this work, we will focus on the O_2 transition associated with an unperturbed line center at 119 GHz. We choose this line as the basis of further discussion because it is one of the simplest lines available to present the theoretical basis of our method. The unperturbed line strength is divided between three perturbed lines. There is still a line at the unperturbed line center carrying the original line strength but for only one linear polarization. We will denote the polarization associated with this perturbed line as horizontal. The other two lines are displaced by approximately ± 14 Hz/nT relative to the unperturbed line center. These are each associated with one type of circular polarization, and both are associated with the remaining linear polarization. The circular polarizations are from here on referenced as right circular and left circular, respectively. The linear polarization associated with these perturbed lines is referenced as vertical from here on. Note that an angular change of 180° for the magnetic field will switch which line carries what circular polarization but will not affect the linear polarization order at all. For other Zeeman-affected transitions, the energy perturbation scheme may be more complex, but it should be possible to translate all results herein with relative ease [*Schadee*, 1978; *Berestetskii et al.*, 1980].

[9] The relative shift of the perturbed lines is very small on Mars for realistic magnetic field strengths. The pressure and Doppler broadening widths are usually much larger, though with a field of 10,000 nT, the Doppler broadening is on the same order of magnitude as the Zeeman shift for the 119 GHz line. This might create the impression that the Zeeman signal is often hidden from spectroscopic analysis. We intend to show, both through simulations and simplified analytical representation of the line cross section, that this is not necessarily the case. It should on the contrary be possible for instruments with frequency resolution on the order of the Doppler broadening width to detect the signal associated with the Zeeman effect. We furthermore suggest that the magnetic field is a necessary adjustable parameter for analysis of Mars O_2 signals by instruments with high-frequency resolution and that the strength of the southern magnetic anomalies can be inferred from the difference between the two perpendicular linearly polarized components of such a signal.

2.2. The Polarized Line Shape

[10] We take a closer look at the line shape associated with any line center in an atmosphere in order to explain the results. The Faddeeva function describes the shape of the line as a function of pressure and temperature around a line center [e.g., *Sampoorna et al.*, 2007]. The Faddeeva function is

$$w(z) = e^{-z^2}\,\mathrm{erfc}(-iz), \tag{1}$$

where $z = \nu' + ia$, and

$$\nu' = \frac{\nu - \nu_0 - \Delta\nu_0}{\Delta\nu_D}, \quad a = \frac{\Delta\nu_p}{\Delta\nu_D}. \tag{2}$$

[11] In the equations above, $\mathrm{erfc}(-iz)$ is the complex error function, ν is the frequency variable, ν_0 is the frequency of the unperturbed line center, $\Delta\nu_0$ is the Zeeman frequency shift relative to the line center, $\Delta\nu_D$ is the Doppler broadening width, and $\Delta\nu_p$ is the pressure broadening width. The real part of the Faddeeva function is associated with attenuation and the imaginary part is associated with dispersion. A combination of the real and imaginary part can be used to describe line mixing in the theory of pressure broadening [see, e.g., *Baranger*, 1958; *Fano*, 1963]. We ignore line mixing by choosing the isolated 119 GHz line where we know the effect is negligible near the line center at low pressures (from, e.g., *Makarov et al.* [2011], the effect decreases linearly with pressure). Although the phase is important when considering propagation of the radiation through a medium with a complicated magnetic field, we will only discuss attenuation below since we think this is enough to demonstrate the method.

[12] A single line will have its signal strength distributed as described by equation (1). The Zeeman effect will cause

a change in the line shape by addition from each contributing perturbed line center. Thus, a single linearly polarized sensor expects $w(z_\pi)$, $[w(z_{\sigma_-}) + w(z_{\sigma_+})]/2$, or any mixing of these two to be the result of its measurements. Here $w(z_\pi)$ represents the shape of the central line and $w(z_{\sigma_\pm})$ the respective outer line shapes. The line strength is equally distributed between the perturbed components, i.e., the total cross section is

$$\sigma_I = \frac{1}{2}\left[\sin^2(\theta) w(z_\pi) + (1+\cos^2\theta)\frac{w(z_{\sigma_-}) + w(z_{\sigma_+})}{2}\right], \quad (3)$$

where θ is the angle of propagation of the radiation and the magnetic field. The data from *Hartogh et al.* [2010] inherently represent total intensity by averaging two perpendicular linear polarizations. Our interpretation is that this approach leaves largely unconstrained conditions in analysis up to the modeler, when the Zeeman effect is significant. Essentially, the modelers may alter either the magnetic field or the atmosphere to produce similar effects in the final results and must use their best judgment to determine what is reasonable. For instance, a different temperature profile in the atmosphere, or a different vertical O_2 distribution, may produce the same results in a model as the Zeeman effect would do. A better approach is to allow for the separation of the Zeeman effect from other atmospheric effects, e.g., by measuring the difference between the perpendicular linear polarizations, i.e., utilize the linearly polarized cross-section shape

$$\sigma_Q = \frac{\sin^2(\theta)\cos 2\eta}{2}\left[\frac{w(z_{\sigma_-}) + w(z_{\sigma_+})}{2} - w(z_\pi)\right], \quad (4)$$

where η is the anticlockwise angle between the axis of the vertical polarization component and the magnetic field projected on the plane defined by the propagation direction. Regardless of the geometry, a nonzero σ_Q contains some magnetic contribution for a given atmospheric level. Combining this with the information from σ_I, i.e., through $\sigma_I \pm \sigma_Q$, provides the modeler with better constraints when estimating the atmospheric parameters. Note that a linear polarization measurement will only experience $\sigma + \sigma_Q$ or $\sigma_I - \sigma_Q$. Also note that the expected cross section for the total intensity when the Zeeman effect is ignored is $w(z_\pi)$ for both linear polarization components, which are then centered at ν_0. The expected cross-sectional residual from models ignoring the Zeeman effect is then $(1+\cos^2\theta)\sigma_Q(\theta = 90°, \eta = 0°)$. This means that the Zeeman effect is seen even in polarization independent measurements and that only if the residual of σ_I is σ_Q for magnetically affected measurements may we know the orientation. Otherwise, a nonzero σ_Q means that $|\theta|$ and η may be estimated from the residual above. This better constrains the problem of the magnetically dependent line shape, although it still leaves some interpretation up to the modeler. We will assume an idealized geometry for the strongest possible linearly polarized cross section, $\theta = 90°$ and $\eta = 0°$, for most of the discussion that follows.

[13] It is clear that the exponential of equation (1) contributes greatly to the drop-off rate of the shape function. With two closely adjacent, but oppositely polarizing lines, this can be used to approximate at which frequency one or the other polarization is dominant; the vertical polarization will dominate as the horizontal polarization decreases with increasing z^2. We already know that the horizontal polarization signal will be strongest close to the unperturbed line center. Assuming the change in main polarization occurs at $\mathrm{Re}(z^2) \approx 1$, we can say that the vertical polarization extrema of equation (4) occurs at

$$\nu_{\max} \approx \nu_0 \pm \sqrt{(\Delta\nu_D)^2 + (\Delta\nu_p)^2}. \quad (5)$$

[14] Equation (5) is derived with $|\Delta\nu_0| \ll \sqrt{(\Delta\nu_D)^2 + (\Delta\nu_p)^2}$ as the limit, and the peaks of σ_Q are otherwise found at $\nu_0 \pm \Delta\nu_0$. If we are within the limits of equation (5), the magnetic field may be determined from σ_Q at $\nu_{\max}$ and at ν_0.

[15] Despite our focus on linear polarization above, the results of equation (5) also apply for circular polarization. In this case, the perturbation from the Zeeman effect is twice as large, which might make it seem that the signal should be noticeable for even weaker magnetic fields with circular polarization than with linear polarization. This is indeed the case for all individual layers. There is, however, one major complication with using a circularly polarized sensor if the magnetic field direction changes strongly over relatively short distances. It is possible, e.g., in limb sounding, that the circular polarization order changes throughout the propagation path. This may essentially negate all information in the signal except for the broadening contributions at $\nu_{\max}$.

3. Results and Discussion

[16] Our modeled level-by-level relative polarized cross section σ_Q of the Zeeman effect signal for the 119 GHz O_2 line on Mars is shown in Figure 1a for various magnetic field strengths. Atmospheric conditions have been taken from a Mars climatology data set compiled for a planetary propagation toolbox [*Rezac and Mendrok*, 2012] and provided with the ARTS radiative transfer model [*Buehler et al.*, 2005; *Eriksson et al.*, 2011], where mean conditions including pressure altitude and temperature were derived from the Laboratoire de Meterologie Dynamique (LMD) Global Circulation Model [*Forget et al.*, 1999]. *Brain et al.* [2003] modeled 15,800 nT as the highest field strength at Mars, but this value could also be "as high as 19,900 nT under certain assumptions" (D. Brain, private communications, 2013).

[17] Figure 1b show us the frequency shift of the outer peaks of σ_Q. For weak magnetic fields and low pressures, these peaks are indeed found at $\nu_{\max} - \nu_0 \simeq \Delta\nu_D$ from the line center, as can be predicted from Equation 5. An instrument capable of measuring the Zeeman effect on Mars must have a frequency resolution of the order of $\Delta\nu_D$. Significantly better frequency resolution than $\Delta\nu_D$ is not necessary to facilitate detection since the difference between horizontal and vertical polarization around $\Delta\nu_D$ should be sufficient to determine the magnetic field. Instruments capable of this frequency resolution today include those presented by *Hartogh et al.*, 2009 and *Murtagh et al.* [2002]. If a copy of one of these instruments was placed in orbit around Mars, we think it would be able to map the magnetic field at middle to high altitudes, although such a copy of the Odin-SMR instrument must be altered to allow measurement of a secondary linear polarization. A somewhat similar instrument design for a Mars mission has been proposed by *Kasai et al.* [2012], though their work does not explicitly mention the goal of measuring O_2 lines.

[18] We find from Figure 1a that a signal-to-noise-ratio of about 100 is required to detect and quantify a 1000 nT strong

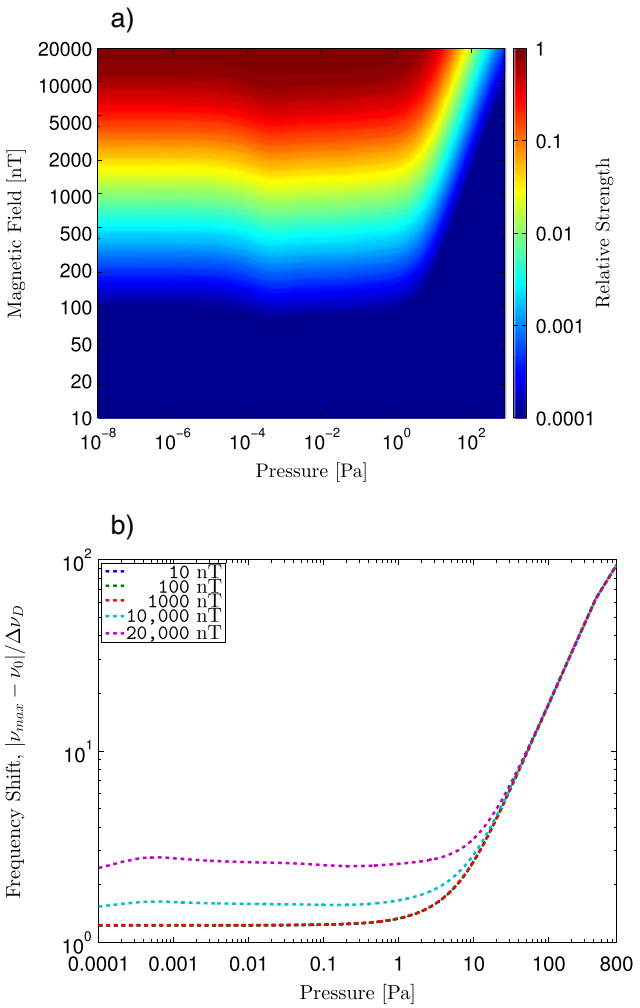

Figure 1. Relative polarized cross-sectional differences between two perpendicular linear polarizations as a function of pressure and range of possible magnetic field strengths at Mars for the 119 GHz O_2line. Figure (a) is $|\sigma_Q|_{\max}$, where the relative numerical values are compared with $w(z_\pi)$ at $\nu = \nu_0$. Figure (b) shows the frequency shift ($\nu_{\max} - \nu_0$), in Doppler broadening widths, of the outer extrema of σ_Q at Mars for the 119 GHz O_2 line. Note that the absolute relative signal strength increases linearly in the logarithmic plane with increasing magnetic field strength inside the limits of equation (5).

magnetic field at heights above 10 Pa. Below 100 Pa, the relative strength is significantly reduced for magnetic fields of the same order. Considering a mean Martian surface pressure of ∼800 Pa, stronger fields ($\gtrsim$10,000 nT) may be detectable at the surface, though the peak of σ_Q will be shifted closer to $100\Delta\nu_D$. The signal strength will be significantly reduced, however, so near-surface magnetic fields can probably not be mapped with the described line method for reasonable integration times.

[19] Extrapolation of the 119 GHz results to the 774 GHz O_2 line measured by *Hartogh et al.* [2010] is possible with some adjustments. The most significant change is that the maximum perturbation is at about ±50 Hz/nT from the line center. The larger frequency perturbation is due to the different type of transition. Following *Berestetskii et al.* [1980], transitions of the type $\Delta J = 0$ and $\Delta N = \pm 2$, which is the case for the 774 GHz line, will be more perturbed than transitions of the type $\Delta J = \pm 1$ and $\Delta N = 0$, as is the case for the 119 GHz line. In this example, N is the quantum number associated with total angular momentum disregarding spin and J is the quantum number taking spin into account for the total angular momentum. The Zeeman effect signal should thus be more easy to detect at 774 GHz, compared to at 119 GHz. We simulated measurements for a simplified radiative transfer scenario in ARTS to emulate the results of *Hartogh et al.* [2010] for an ideal and constant magnetic field (see supporting information). This simplified scenario yields that a magnetic field strength of 10,000 nT should be able to explain most of the residual in Figure 4 (lower panel) of *Hartogh et al.* [2010]. However, the atmospheric profile and the magnetic fields in this approach were both assumed constant. The magnetic field should be stronger closer to the surface, where most of the O_2 signal originates. Most of the polarization difference around $\Delta\nu_D$, however, occurs at higher altitudes. Due to the logarithmically increasing signal strength with increasing magnetic field strength, a single volume with a field strength of 20,000 nT should contribute about 10 times more to the signal than twice the volume with a field strength of 10,000 nT. This means that the contribution from a single strong source may be able to significantly change the shape of the overall signal.

[20] Let us now leave Mars and turn to the subject of exoplanets. Detection of magnetization on exoplanets is still a field in its infancy. However, considering Mars as a proxy for weakly magnetized terrestrial planets outside the solar system, some remarks can be made from our analysis. Following Figure 1a, it is easier to detect a weak magnetic field on an exoplanet with a cold lower atmosphere, compared to a warmer equivalent. This is because the relative strength increases logarithmically not only with increasing magnetic field but also with decreasing Doppler broadening.

[21] Current methods for detection of exoplanets are biased toward detection of big planets in close orbits around their parent stars, i.e., gas giants with relatively high equivalent temperatures. However, the long-term operation of the Kepler telescope, in conjunction with technical improvements for radial-velocity follow-up as well as direct imaging/measurements, should generate a host of suitable colder terrestrial candidates for remote detection of magnetic fields in the near future.

4. Conclusions

[22] It should be possible to isolate the signal generated by the Zeeman effect by measuring the difference between two perpendicularly polarized signals around O_2 lines on Mars. Two perpendicular linearly polarized sensors with frequency resolution on the order of $\Delta\nu_D$ around an unperturbed line center can be used to isolate the Zeeman effect from the remaining signal and allow quantification of the magnetic field. An added benefit of such an analysis would be better constraints on estimation of other atmospheric parameters. A cooled limb-sounding sensor should be able to map the magnetic field above 20 km on Mars for weaker magnetic fields. For stronger localized magnetic fields, this method should allow mapping at altitudes close to the surface.

[23] An average Martian magnetic field of 10,000 nT could explain significant parts of the residual associated with

the measurements-analysis comparison by *Hartogh et al.* [2010]. However, it is impossible to quantify the effects of the magnetic anomalies without further analysis of the unreduced spectral data, and even then it would be very difficult. Given the magnetic field model provided by *Brain et al.* [2003], it is difficult to estimate how large volumes of the Martian lower atmosphere carry 10,000 nT strong magnetic fields, though from our radiative transfer model, it should be clear that a few isolated stronger fields may contribute significantly more to the signal than their average geographical distribution implies.

[24] If a suitable exoplanet is found and the background noise can be kept sufficiently low, we suggest to attempt the method described in this paper in order to detect magnetization on the planet.

[25] **Acknowledgements.** The authors are thankful to Dave Brain for communications about the surface magnetic field on Mars. The authors are also thankful to Paul Hartogh for discussions about the measurements of Mars O_2 by Herschel. Finally, the authors are grateful to the larger ARTS community for development and distribution of the model.

[26] The Editor thanks two anonymous reviewers for their assistance in evaluating this paper.

References

Barabash, S., A. Fedorov, R. Lundin, and J. Sauvaud (2007), Martian atmospheric erosion rates, *Science*, *315*, 501–503.

Baranger, M. (1958), Problem of overlapping line in the theory of pressure broadening, *Phys. Rev.*, *111*(2), 494–504.

Berdyugina, S. V., and S. K. Solanki (2002), The molecular Zeeman effect and diagnostics of solar and stellar magnetic fields—I. Theoretical spectral patterns in the Zeeman regime, *Astron. Astrophys.*, *385*, doi:10.1051/0004-6361:20020130.

Berestetskii, V. B., E. M. Lifshitz, and L. P. Pitaevskii (1980), *Landau and Lifshitz Course of Theoretical Physics: Quantum Electrodynamics*, vol. 4, 2nd ed., Pergamon Press, Oxford, U. K.

Brain, D. A., F. Bagenal, M. H. Acuña, and J. E. P. Connerney (2003), Martian magnetic morphology: Contribution from the solar wind and crust, *J. Geophys. Res.*, *108*, 1424, doi:10.1029/2002JA009482.

Buehler, S. A., P. Eriksson, T. Kuhn, A. von Engeln, and C. Verdes (2005), ARTS, the atmospheric radiative transfer simulator, *J. Quant. Spectrosc. Radiat. Transfer*, *91*(1), 65–93, doi:10.1016/j.jqsrt.2004.05.051.

Citron, R. I., and S. Zhong (2012), Constraints on the formation of the Martian crustal dichotomy from remnant crustal magnetism, *Phys. Earth Planet. Inter.*, *212–213*, 55–63.

Eriksson, P., S. A. Buehler, C. P. Davis, C. Emde, and O. Lemke (2011), ARTS the atmospheric radiative transfer simulator, version 2, *J. Quant. Spectrosc. Radiat. Transfer*, *112*(10), 1551–1558, doi:10.1016/j.jqsrt.2011.03.001.

Fano, U. (1963), Pressure broadening as a prototype of relaxation, *Phys. Rev.*, *131*(1), 259–268.

Forget, F., F. Hourdin, R. Fournier, C. Hourdin, O. Talagrand, M. Collins, S. R. Lewis, P. L. Read, and J.-P. Huot (1999), Improved general circulation models of the Martian atmosphere from the surface to above 80 km, *J. Geophys. Res.*, *104*(10), 24,155–24,176.

Haider, S. A., K. K. Mahajan, and E. Kallio (2011), Mars ionosphere: A review of experimental results and modeling studies, *Rev. Geophys.*, *49*, RG4001, doi:10.1029/2011RG000357.

Hartmann, G. K., et al. (1996), Zeeman splitting of the 61 gigahertz oxygen (O_2) line in the mesosphere, *Geophys. Res. Lett.*, *23*(17), 2329–2332.

Hartogh, P., et al. (2009), Water and related chemistry in the solar system. A guaranteed time key programme for Herschel, *Planet. Space Sci.*, *57*, 1596–606, doi:10.1016/j.pss.2009.07.009.

Hartogh, P., et al. (2010), Herschel/HIFI observations of Mars: First detection of O_2 at submillimetre wavelengths and upper limits on HCl and H_2O_2, *Astron. Astrophys.*, *521*, L49.

Hunten, D. M. (1993), Atmospheric evolution of the terrestrial planets, *Science*, *259*, 915–920.

Jefferies, J., B. W. Lites, and A. Skumanich (1989), Transfer of line radiation in a magnetic field, *Astrophys. J.*, *343*, 920–935.

Kasai, Y., et al. (2012), Overview of the Martian atmospheric submillimetre sounder FIRE, *Planet. Space Sci.*, *291*(5510), 62–82, doi:10.1016/j.pss.2011.10.013.

Kasting, J. F. (1993), Earth's early atmosphere, *Science*, *259*, 920–926.

Lenoir, W. B. (1967), Propagation of partially polarized waves in a slightly anisotropic medium, *J. Appl. Phys.*, *38*(13), 5283–5290.

Lundin, R., S. Barabash, M. Yamauchi, H. Nilsson, and D. Brain (2011), On the relation between plasma escape and the Martian crustal magnetic field, *Geophys. Res. Lett.*, *38*, L02102, doi:10.1029/2010GL046019.

Makarov, D. S., M. Y. Tretyakov, and P. W. Rosenkranz (2011), 60-GHz oxygen band: Precise experimental profile and extended absorption modeling in a wide temperature range, *J. Quant. Spectrosc. Radiat. Transfer*, *112*, 1420–1428.

Murtagh, D., et al. (2002), An overview of the Odin atmospheric mission, *Can. J. Phys.*, *80*(4), 309–319, doi:10.1139/P01-157.

Nilsson, H., N. J. Edberg, G. Stenberg, S. Barabash, M. Holmstrm, Y. Futaana, R. Lundin, and A. Fedorov (2011), Heavy ion escape from Mars, influence from solar wind conditions and crustal magnetic fields, *Icarus*, *215*(2), 475–484, doi:10.1016/j.icarus.2011.08.003.

Rezac, L., and J. Mendrok (2012), Microwave propagation toolbox for planetary atmospheres—Technical note 2 (d3): Atmospheric characterisation technical details and expected accuracy, *Tech. rep.*, ESTEC Contract No 4000104175/11/NL/AF.

Sampoorna, M., K. N. Nagendra, and H. Frisch (2007), Generalized Voigt functions and their derivatives, *J. Quant. Spectrosc. Radiat. Transfer*, *104*, 71–85.

Schadee, A. (1978), On the Zeeman effect in electronic transitions of diamotic molecules, *J. Quant. Spectrosc. Radiat. Transfer*, *19*, 517–531, doi:10.1016/0022-4073(78)90020-1.

Schwartz, M. J., W. G. Read, and W. V. Snyder (2006), EOS MLS forward model polarized radiative transfer for Zeeman-split oxygen lines, *IEEE Geosci. Remote Sens. Lett.*, *44*(5), 1182–1191, doi:10.1109/TGRS.2005.862267.

Seki, K., R. C. Elphic, M. Hirahara, T. Terasawa, and T. Mukai (2001), On atmospheric loss of oxygen ions from Earth through magnetospheric processes, *Science*, *291*(5510), 1939–1941, doi:10.1126/science.1058913.

Selsis, F., J. F. Kasting, B. Levrard, J. Paillet, I. Ribas, and X. Delfosse (2007), Habitable planets around the star Gliese 581?, *Astron. Astrophys.*, *476*, 1373–1387, doi:10.1051/0004-6361:20078091.